UDK 669.017.12:621.74
Original scientific article/Izvirni znanstveni članek

ISSN 1580-2949
Mater. Tehnol.

HETEROGENOUS EQUILIBRIA IN Al-Mn QUASICRYSTALLINE ALLOY DURING HIGH-PRESSURE DIE CASTING

HETEROGENA RAVNOTEŽJA V Al-Mn KVAZIKRISTALNI ZLITINI MED VISOKOTLAČNIM LITJEM

Borut Dremelj[1], Adam Zaky[2], Iztok Naglič[2], Matej Zupančič[2], Boštjan Markoli[2]

[1]LTH Castings d.o.o., Slovenia
[2]University of Ljubljana, Faculty of Natural Sciences and Engineering, Slovenia

Prejem rokopisa – received: 2026-03-18; sprejem za objavo – accepted for publication: 2026-04-15

doi:10.17222/mit.2026.1703

Using advanced characterization techniques, including optical microscopy, scanning electron microscopy (SEM) with energy-dispersive spectroscopy (EDS), and differential scanning calorimetry (DSC) combined with Thermo-Calc calculations, the study demonstrated the relationship between casting conditions, microstructure, and phase formation during high-pressure die casting (HPDC) and comparative gravity casting in steel and copper molds. We demonstrated how both casting conditions and changes in the alloy's chemical composition instigate different heterogeneous equilibria and thus influence the constitution of the alloys. After equilibrium solidification, the microstructures of the synthesized alloys consist of α_{Al} matrix, Al_6Mn, and traces of Al_2CuMg, $Al_{12}Mn$, and Mg_2Si, while nonequilibrium solidification led to the formation of different phases, such as icosahedral quasicrystalline (IQC) phases, such as icosahedral quasicrystalline (IQC) phases their approximant α-AlMnSi and β-AlMnSi phase. Finally, we confirmed the presence of different heterogeneous equilibria that existed simultaneously during the solidification of the investigated alloys.

Keywords: Al-alloys, quasicrystals, equilibrium, HPDC

Z uporabo sodobnih metod karakterizacije, vključno z optično mikroskopijo, vrstično elektronsko mikroskopijo (SEM) in energijsko disperzijsko spektroskopijo (EDS) ter diferencialno vrstično kalorimetrijo (DSC) v kombinaciji s Thermo-Calc izračuni, je v študiji prikazana povezava med pogoji litja, mikrostrukturo in nastankom faz pri visokotlačnem litju (HPDC) ter primerjalnem gravitacijskem litju v jeklene in bakrene kokile. Pokazano je, da tako pogoji litja kot spremembe kemične sestave zlitine sprožijo različna heterogena ravnotežja in s tem vplivajo na sestavo zlitin. Po ravnotežnem strjevanju so mikrostrukture sintetiziranih zlitin sestavljene iz prevladujoče matrice α_{Al} in Al_6Mn ter sledov Al_2CuMg, $Al_{12}Mn$ in Mg_2Si, medtem ko se med neravnotežnim strjevanjem formirajo nove faze, kot so ikozaedrična kvazikristalna faza (IQC) in njen aproksimant α-AlMnSi in faza β-AlMnSi. Potrdili smo prisotnost različnih heterogenih ravnotežij, ki so obstajala hkrati med strjevanjem preiskovanih zlitin.

Ključne besede Al-zlitine, kvazikristali, ravnotežje, visokotlačno litje

1 INTRODUCTION

Alloys capable of forming quasicrystals have been studied since Shechtman's discovery of quasicrystals in Al-Mn alloys in 1986.[1] Many researchers have shown that quasicrystals can form in various alloys and at different cooling rates.[2–13] Recently, significant effort has focused on making these alloys more practical and applicable. The latest research indicates that both the chemical composition of alloys and casting conditions are crucial in controlling microstructure evolution during solidification.[14,15] Dubois et al. presented a compendium summarizing the current state of applications of quasicrystal-forming alloys, highlighting ongoing gaps in the research and application, particularly regarding high pressure die casting (HPDC) of these alloys.[8,16,17] During HDPC and related nonequilibrium solidification conditions, heterogeneous equilibria occur, leading to the solidification of typically multicomponent alloys with highly complex constitutions. Therefore, to further elucidate the solidification behaviour of complex Al–Mn-based alloys under HPDC conditions, the present study compares the solidification of complex Al–Mn-based alloys under industrial HPDC conditions and controlled laboratory gravity casting using copper and steel molds.

2 EXPERIMENTAL PART

The alloys were synthesized in a laboratory furnace and an industrial gas furnace. Technically pure aluminum (99.8 *w*/%), copper (99.9 *w*/%), silicon (99.9 *w*/%), iron (99.8 *w*/%), chromium (99.8 *w*/%), and master alloys AlMn20, AlTi10, AlZr10, AlCa8, AlSr10, AlMg50, ferrovanadium (V80Fe20), and AlV10 were used for the synthesis.

First, aluminum was melted in a graphite crucible at approximately 880 °C, then the other elements were added in order of decreasing melting point and solubility in the aluminum melt. The process was accompanied by

*Corresponding author's e-mail:
bostjan.markoli@ntf.uni-lj.si (Boštjan Markoli)

stirring the molten melt and removing the gaseous components and oxide layer.

The alloys, which typically form metastable primary IQC phases during rapid solidification, were cast at temperatures from 880 °C to 950 °C. The cooling rate of a casting with a diameter of 5.5 mm was calculated using a one-dimensional transient heat transfer model and was approximately 500 K/s for all alloys investigated. The liquidus temperature strongly depends on the manganese content. A high manganese content in the alloy also leads to a higher liquidus temperature, according to the Al-Mn-Si phase diagram.[18] The chemical compositions of the investigated alloys are given in **Table 1**. All alloys were cast under laboratory conditions and by an industrial HDPC process.

Table 1: Chemical compositions of the alloys investigated, in wt.%

Alloy	Al	Mn	Si	Cu/Fe	Mg	V/Ti
BIO1	bal	7.7	1.5	3 (Cu)	3	/
QC-2 (HPDC)	bal	4.4	1.6	2.8 (Cu) 0.2 (Fe)	2.1	/
QC-3 (HPDC)	bal	5.1	0.9	2.9 (Cu) 1.9 (Fe)	2.3	1.0 (V)
QC-4 (HPDC)	bal	6.2	1.0	2.6 (Cu) 0.4 (Fe)	1.5	0.5 (V) 0.4 (Ti)
QC-7 (HPDC)	bal	7.4	0.5	2.7 (Cu) 0.3 (Fe)	0	0.5 (V) 0.4 (Ti)

Microstructural investigations were conducted on alloys subjected to three different cooling conditions during solidification, with the DSC analysis being as the fourth reference process. A calculated cooling rate of approximately 500 K/s was achieved by copper mold casting into a round cavity with a diameter of 5.5 mm. A cooling rate of approximately 250 K/s was achieved by gravity die casting into a steel mold with a plate-shaped cavity measuring 90 mm in length, 40 mm in height, and 3 mm in width. A cooling rate of about 100 K/s was achieved by gravity casting into a copper mold with a round cavity of 15 mm diameter. The gravity casting molds are shown in **Figure 1**.

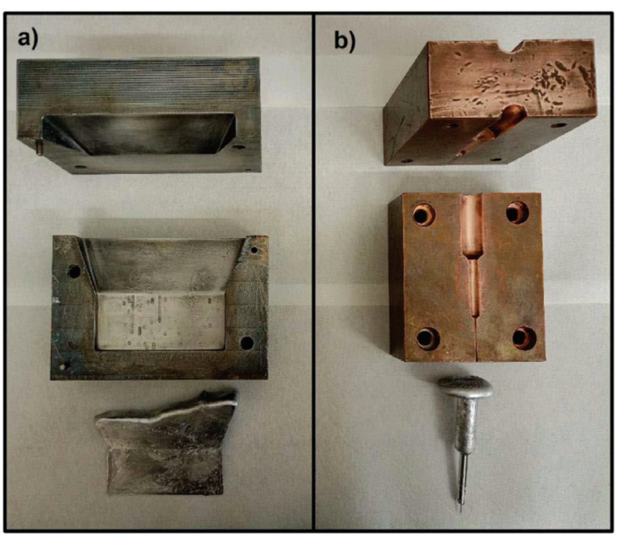

Figure 1: a) Steel and b) copper molds, and corresponding gravity-cast samples with the alloy compositions listed in Table 1

Examination of microstructure evolution during solidification in industrial environments was conducted using a commercial HPDC setup for serial casting of Al-alloys. A NETZSCH Jupiter 449c was used to track the solidification process (differential scanning calorimetry, DSC) of the investigated alloys. Experiments were performed in an Ar atmosphere up to 900 °C, with heating and cooling rates of 10 °C/min. Thermo-Calc software, based on the CALPHAD approach, was used to model the thermodynamic properties of the materials and to forecast the solidification of the investigated alloys. A ZEISS Axio Imager.A1m microscope equipped with an Axiocam 208 color digital imaging camera and ZEN core 3.8 software for image processing and analysis was used for LOM microstructure analysis. For brightfield observation, the specimens were ground and polished with a 0.05 μm silicon oxide suspension for approximately 2 min in the final preparation stage. In some cases, the samples were also etched with a NaOH solution to increase contrast. A Thermo Fisher Quanta 650 scanning electron microscope was used for microstructure observation and microchemical analysis (EDS). Microchemical analyses (EDS) were performed with an Aztec Live Ultim Max SDD 40 mm^2 detector at an acceleration voltage of 20 kV.

3 RESULTS AND DISCUSSION

To determine the solidification behavior of the various alloys listed in **Table 1**, we first examined the equilibrium Thermo-Calc simulations presented in **Figure 2**. The diagrams in the figure clearly show that the solidification path for the investigated alloy BIO1 depends on both manganese content and temperature. On the other hand, we observed that the composition of the investigated alloys is complex and contains numerous phases, some of which are typical for nonequilibrium solidification of Al-based alloys. Based on the chemical composition of BIO1, Thermo-Calc calculated several phases that could form during stable or equilibrium solidification. Primary solidification begins with β-AlMnSi at 810 °C, followed by α-AlMnSi, α_{Al}, Al_6Mn, Al_2CuMg, $Al_{12}Mn$, and Mg_2Si. Stable phase diagrams as a function of temperature and Mn content are shown in **Figure 2**.

We also performed differential scanning calorimetry on the BIO1 sample to obtain detailed information about the thermal processes occurring in a 5.5 mm diameter casting sample from 900 °C to room temperature. Due to metastable or nonequilibrium solidification, the phase composition predicted by the Thermo-Calc software does not fully correspond to the experimentally observed phases, as the software is based on thermodynamic data of stable phases (**Figure 3**). Nevertheless, we established that during cooling (**Figure 3b**), at least four distinct

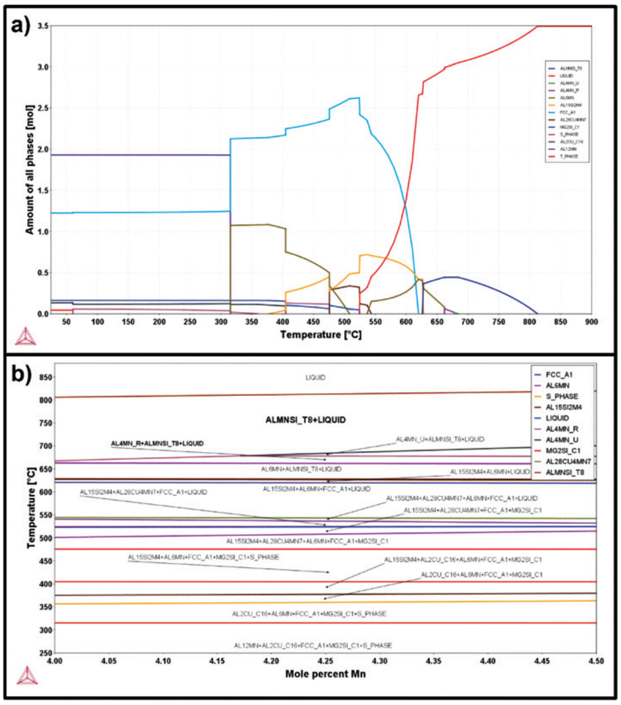

Figure 2: Thermodynamic calculations using Thermo-Calc software: a) predicted phase fraction as a function of temperature, b) solidification temperatures as a function of Mn content

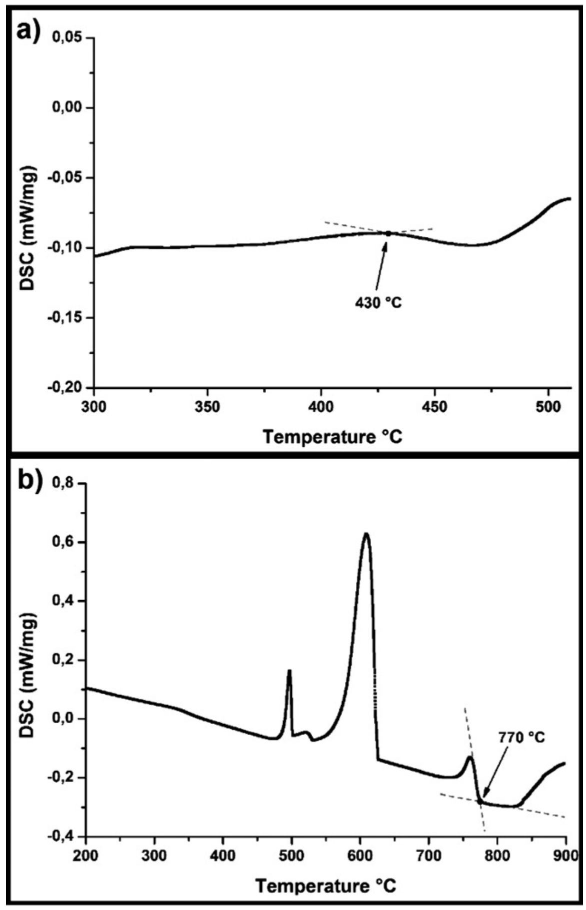

Figure 3: a) DSC heating curve, b) DSC cooling curve of the BIO1 alloy

peaks appeared, corresponding to the primary crystallization of β-AlMnSi at 770 °C, followed by dominant crystallization of the α_{Al} phase at approximately 625 °C. Solidification continued with the formation of heteroge-

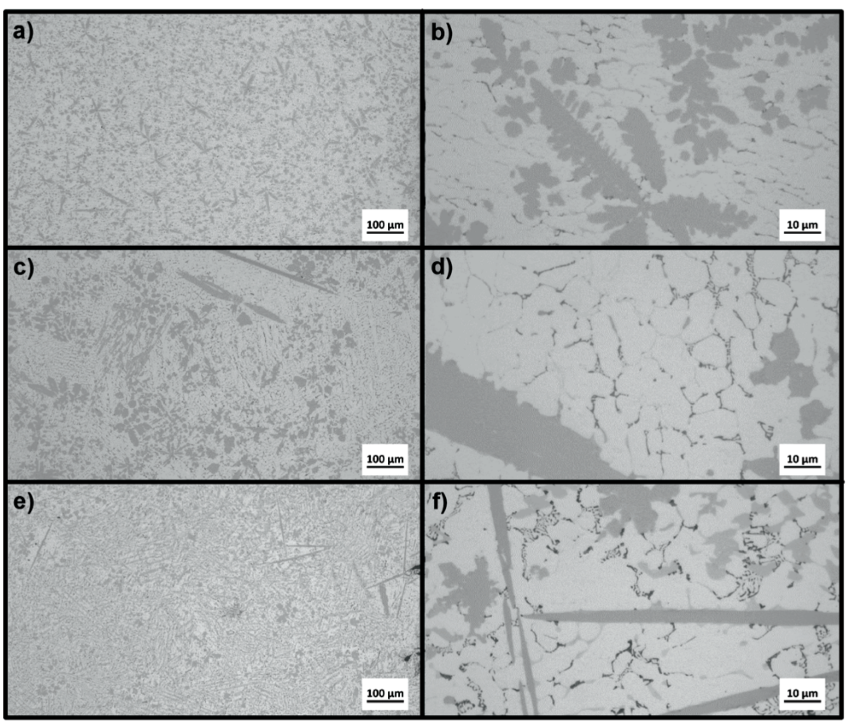

Figure 4: Microstructure of the BIO1 alloy in the central area of the gravity cast samples: a, b) cast in a copper mold with a 5.5 mm diameter cavity; c, d) cast in a copper mold with a 15 mm diameter cavity; e, f) cast in a plate-shaped steel mold, a casting thickness of 3 mm

neous structures consisting of a mixture of β-AlMnSi, α-AlMnSi, and Al_6Mn phases. The discrepancy between the heterogeneous equilibria and the resulting constitution of the investigated alloy as predicted by Thermo-Calc and the actual constitution established during our investigation can be observed.

The presence of the phases described in the previous section was also confirmed by the LOM of the BIO1 alloy, shown in **Figure 4**. The IQC phase, with its typical pentagram or star-like morphology, varies in size from the contact surface between the melt and the inner surface of the casting cavity toward the interior. The occurrence of the long needle-like β-AlMnSi phase becomes more frequent as the casting diameter increases from 5.5 mm to 15 mm. The size of α_{Al} increases noticeably with increasing casting diameter, while the heterogeneous structures between α_{Al} dendrites become coarser and more pronounced due to the reduced solidification rate at the center of a thicker casting. Thus, during the solidification process, the heterogeneous equilibria evolve from the dominant L→IQC phase and L→α_{Al}+IQC into L+β-AlMnSi→α-AlMnSi and L+α_{Al}→ Al_2Cu+Al_6Mn ending with the final L→α_{Al}+Al_2Cu+Mg_2Si+S-phase.

Figures 5 and **6** illustrate the effect of cooling rate on microstructural development in the QC-2 alloy, showing microstructures of the castings produced by gravity casting in copper and steel molds, as well as by HPDC, with significant differences observed between the subsurface and inner regions. In the subsurface region, where cooling and solidification rates are significantly higher (**Figure 5**), IQC particles are sparsely distributed, having star-like morphology, while the remaining constituents form very fine, uniformly sized particles or dendrites, regardless of the casting method. Most importantly, the heterogeneous equilibria evolve, leading to the formation of a new, needle-like morphology of the β-AlMnSi phase.

Further comprehensive DSC analyses of all investigated alloys enabled us to reconstruct the solidification process and establish the heterogeneous equilibria that coexist in the investigated alloys, using a combination of DSC heating and cooling curves, SEM images, and EDS results.

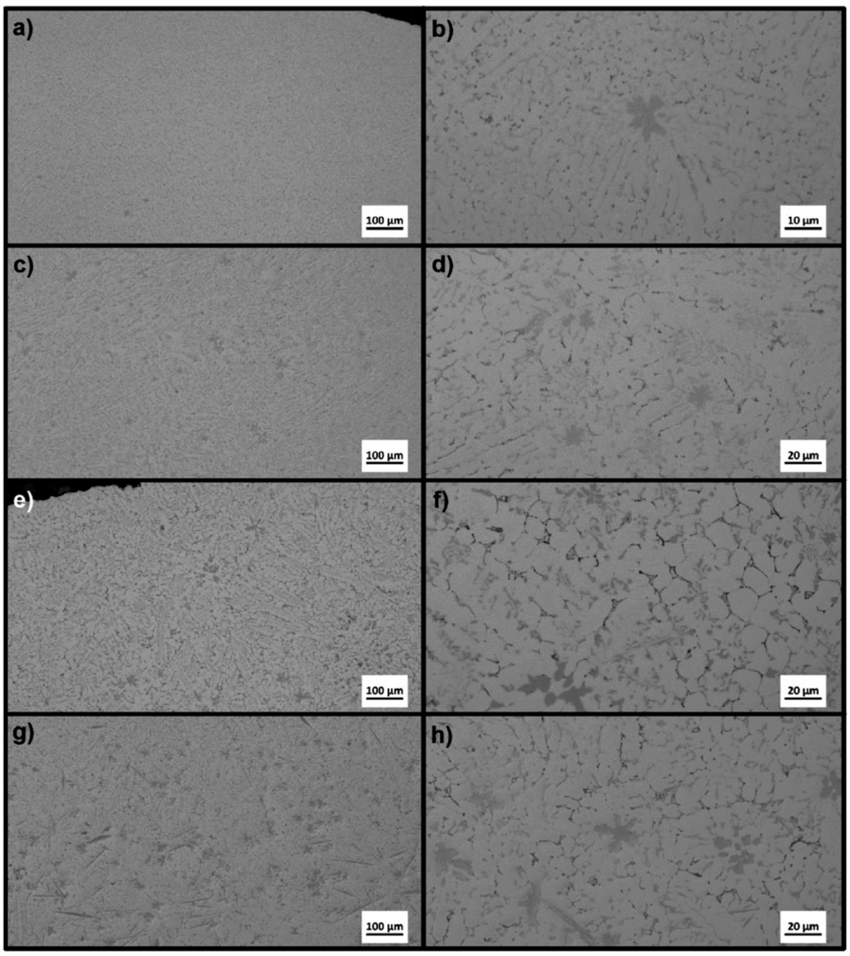

Figure 5: Microstructure of the QC-2 alloy near the contact surface of the gravity and HPDC cast samples: a, b) cast in a copper mold with a 5.5 mm diameter cavity; c, d) cast in a copper mold with a 15 mm diameter cavity; e, f) cast in a shaped steel mold with a thickness of 3 mm; g, h) cast in the HPDC die with a 3 mm thick cavity

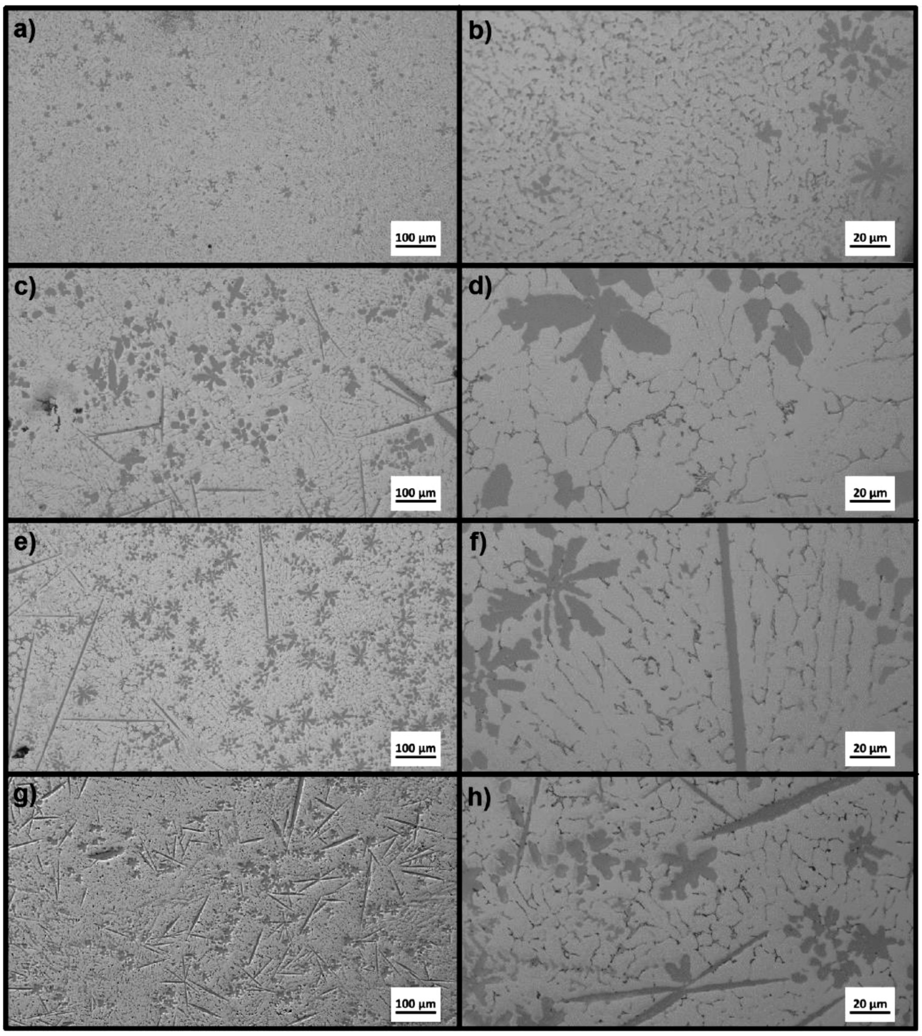

Figure 6: Microstructure of the QC-2 alloy in the central area of the gravity and HPDC cast samples: a, b) cast in a copper mold with a 5.5 mm diameter cavity; c, d) cast in a copper mold with a 15 mm diameter cavity; e, f) cast in a shaped steel mold with a thickness of 3 mm; g, h) cast in

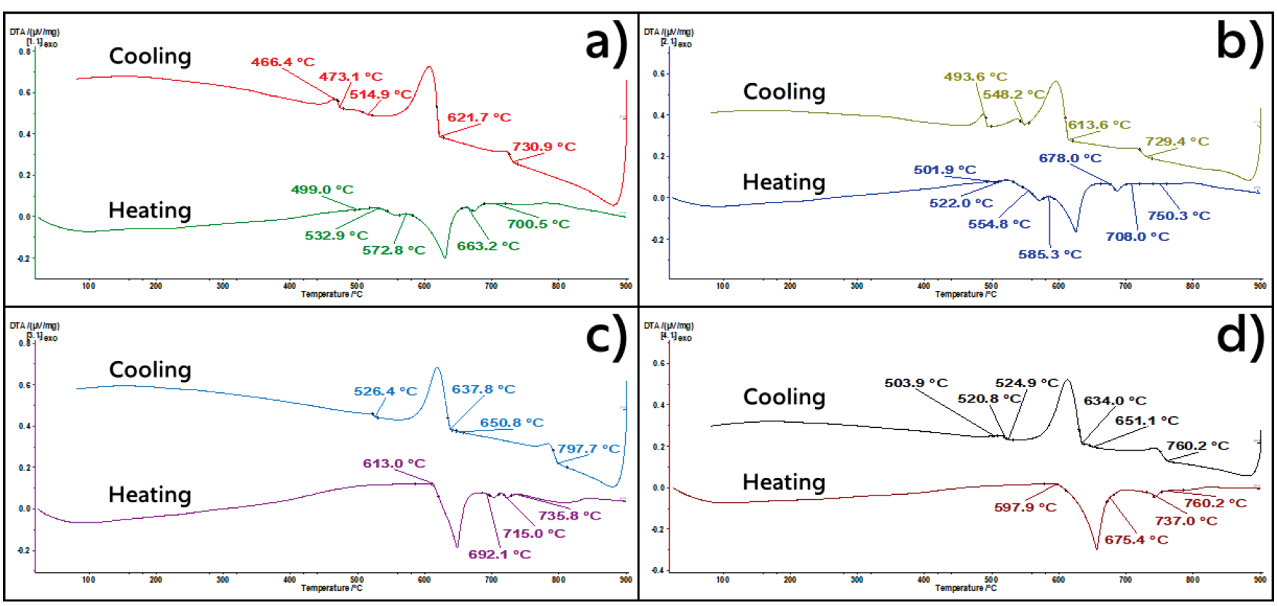

Figure 7: DSC of investigated alloys: a) QC-2, b) QC-3, c) QC-5 and d) QC-7

In **Figure 7**, a collection of DSC heating and cooling curves for all the alloys listed in **Table 1** is presented, illustrating the solidification sequence during DSC analyses.

Significant differences were observed in the intensities of individual DSC peaks. The heating curves showed a considerably narrower solidus–liquidus interval compared to cooling. No corresponding peak temperatures were identified when comparing the heating and cooling curves of the alloys listed in **Table 1**, except for a single case in QC-7 at 760.2 °C. In this instance, primary solidification apparently began with the crystallization of IQC particles exhibiting their characteristic star-like morphology, often accompanied by needle-like quasicrystalline approximants (β-AlMnSi). Differences in size, distribution, and occurrence frequency of microstructural constituents are further evident from the LOM images in **Figure 6**.

The solidification processes of the alloys listed in Table 1 were determined through detailed analyses of DSC curves, combined with the SEM images from **Figure 8**.

There is no evidence of IQC particles in any of the images in Figure 8, which is not surprising, as the formation of quasicrystalline phases requires higher cooling rates than those achieved in DSC, as explained in the Introduction. The primary phase appears as elongated lath-like particles or polygonal bulky particles with a chemical composition close to β-AlMnSi in alloys QC-2

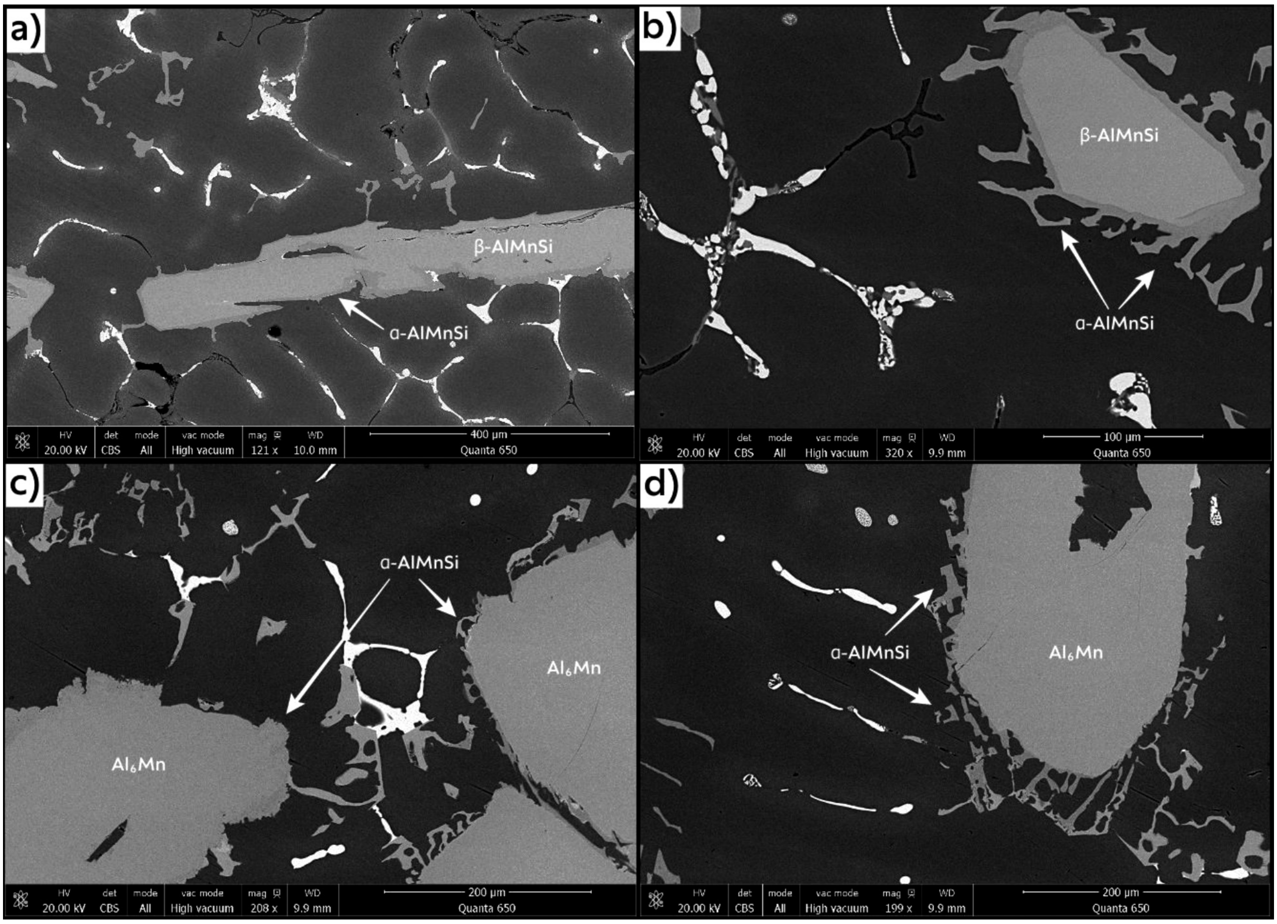

Figure 8: SEM images for a) QC-2, b) QC-3, c) QC-4, d) QC-7 alloys after cooling at 10 °C/min (DSC)

Table 2: Chemical compositions of distinct phases in the investigated alloys obtained using EDS (at.%)

Alloy	Phase	Al	Mn	Si	Fe	Cu
QC-2	β-AlMnSi	69.0	23.0	6.35	0.7	0.15
QC-2	α-AlMnSi	74.5	16.5	8.50	1.0	0.65
QC-3	β-AlMnSi	70.0	22.5	7.00	1.0	0.15
QC-3	α-AlMnSi	74.0	16.0	8.20	1.5	0.30
QC-4	Al_6Mn	81.0	15.5	0.37	1.8	0.38
QC-4	α-AlMnSi	73.0	15.2	7.90	1.5	0.70
QC-7	Al_6Mn	85.0	13.0	0.40	1.6	0.35
QC-7	α-AlMnSi	73.5	16.2	8.05	1.0	1.1

and QC-3, and is surrounded by an outer shell peritectically formed with a composition equal to that of α-AlMnSi. In alloys QC-4 and QC-7, the primary phase changed from ternary β-AlMnSi into one of binary phases, most probably Al_6Mn. This is in accordance with the EDS results from **Table 2**. Solidification then continued in all alloys with the crystallization of α_{Al}, followed by heterogeneous equilibria leading to the formation of binary or ternary eutectic-like structures consisting of Al_6Mn, Al_2CuMg, $Al_{12}Mn$, and Mg_2Si phases, as predicted by Thermo-Calc simulation (**Figure 2**). These phases showed chemical compositions consistent with the EDS microchemical analyses performed using SEM.

Primarily solidified elongated β-AlMnSi or bulky Al_6Mn particles are surrounded by what appears to be a peritectically formed α-AlMnSi phase, rich in both manganese and silicon. We observed that, in the case of primary IQC particles, the α-AlMnSi phase is also peritectically formed on the edges of the IQC phase, which is consistent with the findings of others.[19] Interdendritic spaces are filled with heterogeneous structures, some of which show stronger contrast than others, indicating the presence of copper as confirmed by EDS. Other structures that appear darker or with a grayish contrast have compositions dominated by silicon and/or manganese, belonging to different heterogeneous structures. This is typical of all the alloys investigated, although they have slightly different initial chemical compositions, as shown in **Table 1**. Furthermore, the heterogeneous equilibria leading to the formation of microstructural constituents differ significantly across the four cooling rates employed during our investigation, indicating that cooling rate plays a crucial role in microstructure formation.

4 CONCLUSIONS

Based on the investigation of five different Al-Mn-based alloys employing various cooling rates and small compositional variations, it is possible to significantly influence the course of solidification and, consequently, the final microstructure. This, in turn, can have a profound effect on the properties of the alloys.

We found that the predicted microstructural composition closely matches the composition obtained with DSC analysis. At higher cooling rates, heterogeneous equilibria changed significantly, resulting in the formation of the primary IQC phase, often accompanied by a crystalline approximant based on AlMnSi and other phases typical of the Al-Mn-Si ternary system, such as Al_6Mn, Al_4Mn, and others.

The microstructure also showed significant differences in the size and number of microstructural constituents when observed from the contact surface toward the inner regions of the castings. We also observed that the IQC phase regularly formed as the primary phase when cooling rates were around 400–500 K/s, but was contested by both β-AlMnSi and α-AlMnSi even more dominantly when cooling rates dropped below 300 K/s.

The heterogeneous equilibria established in the investigated alloys during solidification at different cooling rates differed significantly from one another and consistently led to very different constitutions in the alloys studied.

Acknowledgment

Authors would like to acknowledge the support of project No. 21128 A novel cast ultra-high-specific strength quasicrystal aluminum alloy [CastQC], funded by the European Institute of Innovation and Technology.

5 REFERENCES

[1] D. Shechtman, I. Blech, D. Gratias, J. W. Cahn, Metalic Phase with Long-Range Orientational Order and No Translational Symmetry, Physical Review Letters, 53 (**1984**) 20, 1951–1953, doi:10.1103/PhysRevLett.53.1951

[2] L. Battezzati, C. Antonione, F. Marino, Some thermodynamic and kinetic aspects of icosahedral phase nucleation in Al-Mn, Journal of Materials Science, 24 (**1989**) 7, 2324–2330, DOI: doi:10.1007/BF01174491

[3] F. Gillessen, D. Herlach, Nucleation and formation of quasicrystalline phases in undercooled Al-Mn melts, Materials Science and Engineering: A, 134 (**1991**), 1220–1224, DOI: doi:10.1016/0921-5093(91)90960-U

[4] A. McAlister, L. Bendersky, R. Schaefer, F. Biancaniello, Enhanced age-hardening response and creep resistance of an Al-0.5Mn-0.3Si (at.%) alloy by Sn inoculation, Scripta Metallurgica, 21 (**1987**) 2, 103–106

[5] P. A. Bancel, P. A. Heiney, P. W. Stephens, A. I. Goldman, P. M. Horn, Structure of Rapidly Quenched Al-Mn, Physical Review Letters, 54 (**1985**) 22, 2422–2425, doi:10.1103/PhysRevLett.54.2422

[6] F. Schurack, J. Eckert, L. Schultz, Quasicrystalline Al-alloys with high strength and good ductility, Materials Science and Engineering: A, 294 (**2000**), 164–167, doi:10.1016/S0921-5093(00)01191-6

[7] C. Chen, H. Chen, Superlattices in quenched Al-Si-Mn quasicrystals, Physical Review B, 33 (**1986**) 4, 2814, doi:10.1103/PhysRevB.33.2814

[8] J-M. Dubois, Potential and marketed applications of quasicrystalline alloys at room temperature or above, Scienze Fisiche e Naturali, 34 (**2023**), 689–702, doi:10.1007/s12210-023-01170-4

[9] K. Stan-Głowińska, L. Lityńska-Dobrzyńska, J. Morgiel, A. Góral, M. Gordillo, J Wiezorek, Formation of a quasicrystalline phase in Al–Mn base alloys cast at intermediate cooling rates, Journal of Alloys and Compounds, 702 (**2017**), 216–228, doi:10.1007/s10853-017-1011-z

[10] F. Zupanič, G. Lojen, L. Barba, T. Bončina, Effect of Cu on rapidly solidified Al–Mn–Be alloy, Materials Characterization, 70 (**2012**), 48–54, doi:10.1016/j.matchar.2012.05.002

[11] Z. C. Sims, O. R. Rios, D. Weiss, P. E. Turchi, A. Perron, J. R. Lee, T. T. Li, J. A. Hammons, M. Bagge-Hansen, T. M. Willey, High performance aluminum–cerium alloys for high-temperature applications, Materials Horizons, 4 (**2017**) 6, 1070–1078, doi:10.1039/C7MH00391A

[12] A-P. Tsai, A. Inoue, T. Masumoto, A Stable Quasicrystal in Al-Cu-Fe System, Japanese Journal of Applied Physics, 26 (**1987**) 9A, L1505, doi:10.1143/JJAP.26.L1505

[13] A-P. Tsai, New Quasicrystal Approximant in the Sc–Pd System, Chemical Society Reviews, 42 (**2013**) 12, 5352–5365

[14] I. Naglič, B., Leskovar, A. Zaky, B. Arah, J. Sojanović, Ž. Kamberović, P. Boulet, B. Markoli, Influence of copper, calcium and strontium on the formation of quasicrystals in Al-Mn-based alloys, Journal of Alloys and Compounds, 1057 (**2026**), 186847, doi:10.1016/j.jallcom.2026.186847

[15] A. Zaky, B. Leskovar, I. Naglič, B. Markoli, Microstructural characterization of QC-forming Al-Mn-based alloy using machine learning software, JOM, 77 (**2025**) 3, 1123–1132, doi:10.1007/s11837-024-06899-3

[16] J-M. Dubois, Properties- and applications of quasicrystals and complex metallic alloys, Chemical Society Reviews, 41 (**2012**) 20, 6760–6777, doi:10.1039/C2CS35110B

[17] J-M. Dubois, Useful Quasicrystals, World Scientific, London 2005, doi:10.1142/3585

[18] P. Villars, A. Prince, H. Okamoto, Handbook of Ternary Alloy Phase Diagrams, ASM International, 1995

[19] H. J. Chang, E. Fleury, G. S. Song, M. H. Lee, W. T. Kimb, D. H. Kima, Microstructure modification and quasicrystalline phase formation in Al–Mn–Si–Be cast alloys, Materials Science and Engineering A, 375–377 (**2004**), 992–997, doi:10.1016/j.msea.2003.10.004